Journal of Hazardous Materials 446 (2023) 130678

Contents lists available at ScienceDirect

Journal of Hazardous Materials

journal homepage: www.elsevier.com/locate/jhazmat

Research Article

Tracing the transboundary transport of atmospheric Particulate Bound Mercury driven by the East Asian monsoon

Xuechao Qin [a,b,e], Xinyuan Dong [a,b], Zhenghua Tao [a,b], Rongfei Wei [a], Hua Zhang [d], Qingjun Guo [a,c,*]

[a] Center for Environmental Remediation, Institute of Geographic Sciences and Natural Resources Research, Chinese Academy of Sciences, Beijing 100101, China
[b] University of Chinese Academy of Sciences, Beijing 100049, China
[c] College of Resources and Environment, University of Chinese Academy of Sciences, Beijing 100190, China
[d] State Key Laboratory of Environmental Geochemistry, Institute of Geochemistry, Chinese Academy of Sciences, Guiyang 550081, China
[e] Department of Health, Ethics and Society, Care and Public Health Research Institute, Faculty of Health, Medicine and Life Sciences, Maastricht University, Maastricht 6229 HA, the Netherlands

HIGHLIGHTS

- Anthropogenic sources affected the $PBM_{2.5}$ in BTH, identified by Hg and N isotopes.
- East Asian monsoon-driven transport contributed significantly to atmospheric $PBM_{2.5}$.
- Photoreduction of Hg^{2+} during long-range transport led to elevated $\Delta^{199}Hg$ of $PBM_{2.5}$.
- The northwest monsoon from the inland intensified atmospheric $PBM_{2.5}$ pollution.
- The southeast monsoon from the ocean alleviated atmospheric $PBM_{2.5}$ pollution.

GRAPHICAL ABSTRACT

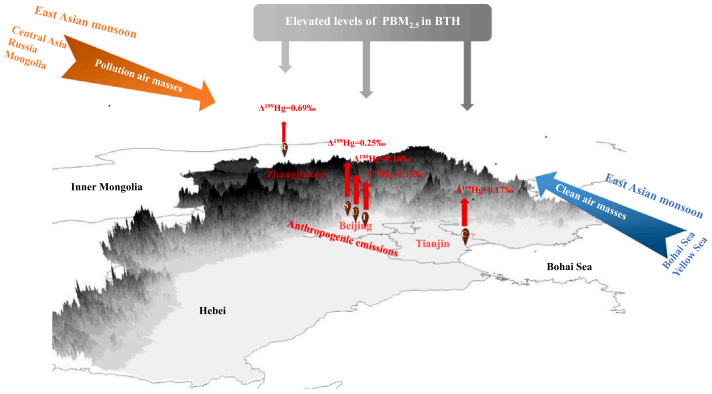

ARTICLE INFO

Keywords:
$PBM_{2.5}$
Mercury isotopes
Mercury circulation
Transboundary transport
East Asian monsoon

ABSTRACT

Taking Beijing-Tianjin-Hebei (BTH) with severe atmospheric mercury (Hg) and $PM_{2.5}$ pollution as a typical region, this study clarified the characteristics and transboundary transport of atmospheric Particulate Bound Mercury ($PBM_{2.5}$) affected by the East Asian monsoon. Five sampling sites were conducted in rural, suburban, urban, industrial, and coastal areas of BTH from northwest to southeast along the East Asian monsoon direction. $PBM_{2.5}$ showed increasing concentrations from northwest to southeast and negative $\delta^{202}Hg$ values, indicating significant contributions from anthropogenic sources. However, the mean $\Delta^{199}Hg$ values of $PBM_{2.5}$ at the five sites were significantly positive, probably triggered by the photoreduction of Hg(II) during long-range transport driven by the East Asian monsoon. Apart from local anthropogenic emissions as the primary sources, the transboundary transport of $PBM_{2.5}$, driven by west and northwest air masses originating in Central Asia and

* Corresponding author at: Center for Environmental Remediation, Institute of Geographic Sciences and Natural Resources Research, Chinese Academy of Sciences, Beijing 100101, China.
E-mail address: guoqj@igsnrr.ac.cn (Q. Guo).

https://doi.org/10.1016/j.jhazmat.2022.130678
Received 29 August 2022; Received in revised form 13 December 2022; Accepted 24 December 2022
Available online 26 December 2022

Russia, contributed significantly to the $PBM_{2.5}$ pollution of BTH. Moreover, these air masses reaching BTH would carry elevated $PBM_{2.5}$ concentrations further transported to the ocean by the East Asian monsoon. In contrast, the southeast air masses transported from the ocean by the East Asian monsoon in summer diluted inland $PBM_{2.5}$ pollution. This study provides insight into the atmospheric Hg circulation affected by the East Asian monsoon.

1. Introduction

Atmospheric mercury (Hg) can be divided into three forms, including gaseous elemental Hg (GEM), gaseous oxidized Hg (GOM), and particulate bound Hg (PBM) [3]. GEM is the dominant form of Hg and has a long-lifetime in the atmosphere, and it can convert to GOM or PBM via various photochemical oxidation or reduction reactions during transport [27,3,78]. Although GOM and PBM account for < 10% of the total atmospheric Hg, due to the high reactivity, they can be quickly removed from the atmosphere by dry or wet deposition in a matter of days to weeks [18,37,41,49]. Once deposited on the earth's surface, Hg can be biologically converted into methylmercury, which may endanger ecology and human health [32,64]. Moreover, PBM can also be produced by various physical or photochemical processes in the atmosphere, such as gas-particle partitioning is a very important atmospheric process controlling PBM levels at local to regional scales [2,3]. In addition, atmospheric particulate matter can act as a carrier of toxic Hg. Of particular concern is the binding of Hg to $PM_{2.5}$ ($PBM_{2.5}$), as both Hg and its particulate matter can adversely affect humans once inhaled.

The East Asian monsoon is one of the largest monsoon zones in the world, covering eastern China, the Korean Peninsula, Japan, and other regions. It manifests as the northwest wind prevails in winter and the southeast wind prevails in summer, significantly impacting atmospheric Hg transport. The global atmospheric Hg emission from anthropogenic activities was about 2500 tons in 2015, a quarter of which was emitted by China [1]. One of the largest Hg emissions areas in China is the Beijing-Tianjin-Hebei (BTH) region, including Beijing, Tianjin, and Hebei province [65]. Moreover, BTH is the area with the most $PM_{2.5}$ pollution of all economic growth poles in China [14]. The combination of Hg and $PM_{2.5}$ in the atmosphere of the BTH region severely threatens both local human and ecological security. The BTH region is greatly affected by the East Asian monsoon. It is an ideal area to study the impact of the East Asian monsoon on atmospheric $PBM_{2.5}$ due to its distinct differences in its natural geographical distribution and diverse landform units, including plateaus, mountains, plains, and coast. For example, Zhangjiakou City, Hebei Province, located in the Yanshan Mountains in the northwest of BTH, is adjacent to Inner Mongolia and less disturbed by human activities. Tianjin, one of China's oldest industrial cities, is near the Bohai Sea in the southeast. Beijing, as the commercial metropolis, is located between the two. However, previous studies on atmospheric $PBM_{2.5}$ have only been conducted in a single city in BTH (mostly in Beijing) [28,44,47,58,60,74,75,77], which is difficult to reveal the characteristics of $PBM_{2.5}$ in BTH and the transport of $PBM_{2.5}$ affected by East Asian monsoons.

Stable isotope analysis is a useful tool for understanding the transport and sources of atmospheric Hg due to its multi-dimensional isotopic signatures, including mass-dependent fractionation (MDF, $\delta^{202}Hg$), odd mass-independent fractionation (odd-MIF, $\Delta^{199}Hg$ and $\Delta^{201}Hg$), and even mass-independent fractionation (even- MIF, $\Delta^{200}Hg$ and $\Delta^{204}Hg$) [12,23,26,4,48]. Both Hg emission sources and atmospheric processes may lead to changes in atmospheric Hg isotopic compositions [12,51,9]. For instance, $PBM_{2.5}$ affected by regional anthropogenic emissions is more likely to preserve the $\Delta^{199}Hg$ value of emission sources, which is generally low and slightly negative [57]. However, $PBM_{2.5}$ with long-range transport would experience more atmospheric processes and transformations so that the $\Delta^{199}Hg$ value positively shifted. [22]. Recently, some studies have used Hg isotopes to reveal how domestic emissions and transboundary Hg transport contribute to atmospheric Hg, though these have mainly been conducted in remote areas [22,25,72]. The situation in the BTH region, however, remains unknown, hindering further understanding of the sources and fate of atmospheric Hg in the region.

In this study, therefore, the BTH region was taken as a typical region to clarify the characteristics and the transport of atmospheric $PBM_{2.5}$ under the influence of East Asian monsoon and landforms using atmospheric $PBM_{2.5}$ isotopes. Since the BTH region is mainly affected by the East Asian monsoon, this study selected five sampling sites from northwest to southeast across the region to collect $PBM_{2.5}$ samples. The five sampling sites are located in Zhangjiakou (Hebei Province), Changping District (Beijing), Chaoyang District (Beijing), Daxing District (Beijing), and Tianjin, respectively. They represent different urban functional areas in the BTH region, namely rural, suburban, urban, industrial (suburban), and coastal (urban) areas, respectively (Fig. 1b). This study thus provides an important opportunity to understand the transport and transformation of atmospheric $PBM_{2.5}$ and the environmental circulation of Hg in regions affected by the East Asian monsoon.

2. Materials and methods

2.1. Sites description

Given the influence of the East Asian Monsoon and diverse landforms on atmospheric $PBM_{2.5}$, $PBM_{2.5}$ samples were collected from five sampling sites from northwest to southeast across the BTH region between December 2016 and November 2017 (Fig. 1b). These sampling sites were located in rural (ZJK, Zhangjiakou city in Hebei province), suburban (CPB, Changping District in Beijing), urban (CYB, Chaoyang District in Beijing), industrial (DXB, Daxing District in Beijing), and coastal (TJ, Binhai New District in Tianjin) areas of the BTH region (Figure1b). Details about these sites are described in Text S1.

2.2. $PM_{2.5}$ sampling and Hg analysis

Atmospheric $PM_{2.5}$ samples were collected from the five sampling sites (ZJK, CPB, CYB, DXB, and TJ) using high-volume samplers (TH-1000 H) with a flow of 1.05 $m^3\ min^{-1}$. Precisely, the air samples flowed through the sampler inlet, the $PM_{2.5}$ separate device, and were captured onto pre-combusted (450 °C for 6 h) quartz fiber filters (20 cm × 25 cm, Munktell, Sweden), while the passing gas was discharged by the exhaust port. In the BTH region, March to May, June to August, September to November, and December to February are spring, summer, autumn, and winter, respectively, and November 15 to March 15 is the heating period. Considering the schedule for heating and seasonal characteristics in the BTH region, we selected December to January (winter), April (spring), July (summer), and November (autumn) from December 2016 to November 2017 as our four sampling periods. The sampling duration of $PBM_{2.5}$ was 24 h. The high-volume samplers used for sampling were stationed approximately 10 m above the ground, and there were no large pollution sources around the sampling sites. During sampling, field blank filters were also collected without air intake. After sampling, the quartz filters were wrapped in aluminum foil, sealed with three successive polyethylene bags, and stored at − 20 °C until analysis.

$PBM_{2.5}$ concentration was determined according to the US EPA method 7473 [59]. In short, the Hg concentration in $PM_{2.5}$ was measured by cold vapor atomic absorption spectrophotometry (CVAAS, Lumex RA915 + coupled with PYRO-915 +) [35,39,50]. The method is to heat the $PBM_{2.5}$ samples at 800 °C to thermally decompose the Hg in the samples to Hg^0 and then measure the released Hg^0 to determine the

$PBM_{2.5}$ concentration. The detection limit of the instrument is 0.1 ng/g. The quality control for this procedure consisted of method blanks, certified reference materials (CRM) GBW07405, and duplicates. The Hg concentration detected in the blank samples was less than 0.25 ng (n = 20), which was lower than 2.5% of the Hg content (>10 ng) in $PM_{2.5}$ samples. Therefore, Hg in the blank samples can be negligible. The average total Hg recovery of CRM GBW07405 was 94 ± 4%(n = 8), and the duplicate sample bias was less than 10%.

2.3. $PBM_{2.5}$ isotopes analysis

A total of 33 $PBM_{2.5}$ samples were selected to determine the isotopic compositions of $PBM_{2.5}$ (Text S2). The $PBM_{2.5}$ samples were pre-concentrated into 5 mL of 40% mixed acid solution using a dual-stage combustion protocol for Hg isotope analysis as described previously [30,53]. $PBM_{2.5}$ isotope ratios were measured by Nu-Plasma MC-ICPMS at the State Key Laboratory of Environmental Geochemistry, Institute of Geochemistry, Chinese Academy of Sciences, following the method described earlier [22,71].

The MDF of $PBM_{2.5}$ isotopes is expressed in delta (δ) notation in units of per mil (‰), and NIST 3133 was used as the reference to calculate the isotopic fractionation [7]:

$$\delta^{xxx}Hg = \left[\frac{\left(^{xxx}Hg/^{198}Hg\right)_{sample}}{\left(^{xxx}Hg/^{198}Hg\right)_{NIST3133}} - 1\right] \times 1000‰ \quad (1)$$

Where xxx = 199, 200, 201, 202, or 204. MIF is represented as the following equation [7]:

$$\Delta^{199}Hg = \delta^{199}Hg - \left(0.252 \times \delta^{202}Hg\right) \quad (2)$$

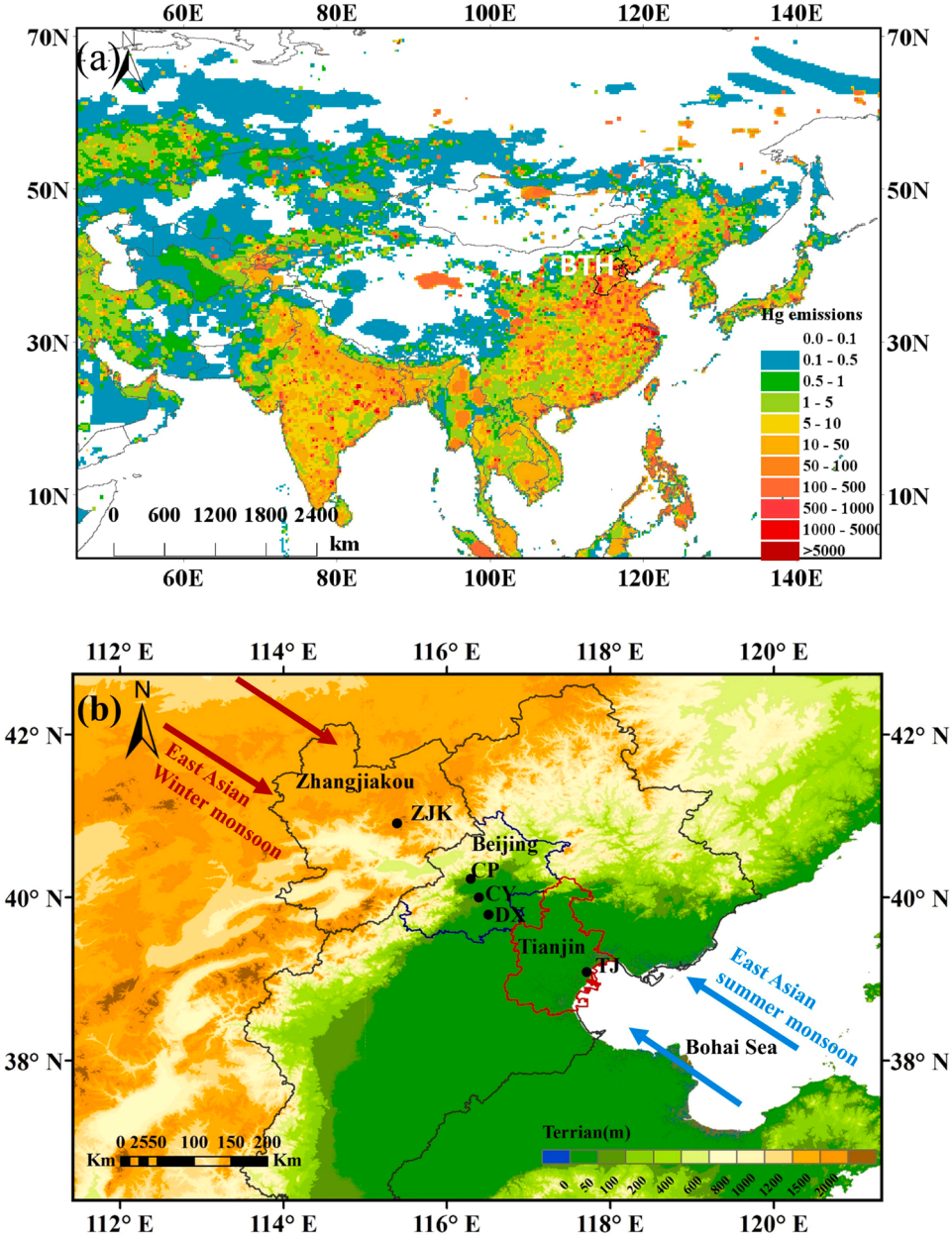

Fig. 1. Anthropogenic total Hg emissions in China (a) and locations of the five sampling sites in the BTH region in our study (b). The gridded data of Hg emissions are from AMAP/UNEP (2019). ZJK, CP, CY, DX, and TJ represent the sampling sites in Zhangjiakou (ZJK), Beijing's Changping (CPB), Chaoyang (CYB), and Daxing districts (DXB), and Tianjin (TJ), respectively.

$$\Delta^{200}Hg = \delta^{200}Hg - (0.502 \times \delta^{202}Hg) \quad (3)$$

$$\Delta^{201}Hg = \delta^{201}Hg - (0.752 \times \delta^{202}Hg) \quad (4)$$

$$\Delta^{204}Hg = \delta^{204}Hg - (1.493 \times \delta^{202}Hg) \quad (5)$$

For quality assurance and control, the average Hg recovery of the dual-stage combustion protocol was analyzed by the CRM GBW07405, which was 99 ± 12% (n = 5). The standard material NIST 8610 was used to analyze the analytical uncertainty during the isotopic analysis session, and the average values of $\delta^{201}Hg$ and $\Delta^{199}Hg$ measured for NIST 8610 were − 0.60 ± 0.10‰ and − 0.02 ± 0.02‰ (2σ, n = 3), which was comparable with previously reported data [68]. The isotopic ratios for each sample were measured only once, so the 2σ uncertainty of NIST 3133 measured repeatedly during the samples analysis session was applied to the samples.

2.4. Ancillary data

Water-soluble anion and cation data in $PM_{2.5}$ samples were taken from our previous study [17]. Daily meteorological data in BTH was taken from the National Meteorological Information Center (http://data.cma.cn/site/index.html). Air quality data, including $PM_{2.5}$, SO_2, etc., were obtained from China National Environmental Monitoring Center (http://www.cnemc.cn/).

The Hybrid Single-Particle Lagrangian Integrated Trajectory (HYSPLIT) model was used to analyze the backward trajectories of air masses at the five sampling sites. Gridded meteorological data were obtained at 4-hour intervals and a resolution of 1° × 1° from the U.S. National Oceanic and Atmospheric Administration (Global Data Assimilation System, GDAS1). The arrival heights and runtime of backward trajectories were 50 m above the ground and 120 h. Based on the HYSPLIT model results and the measured $PBM_{2.5}$ concentrations, the Potential Source Contribution Function (PSCF) model was employed to identify the contribution of each trajectory arriving at the sampling sites and estimate potential sources regions [15]. The PSCF values for grid cells were calculated by computing the endpoints of the trajectory terminating within each cell, and a higher PSCF value indicates a higher potential source contribution to the acceptor sites (Eq. 6):

$$PSCF_{ij} = \frac{M_{ij}}{N_{ij}} W_{ij} \quad (6)$$

where M_{ij} is the total number of these endpoints with $PBM_{2.5}$ concentration in a grid cell (*ij*) above the given criterion value, N_{ij} is the total number of trajectory endpoints in a grid cell (*ij*), and W_{ij} is a weighting function used to adjust for a small number of trajectory endpoints in a grid cell (*ij*) [42].

3. Results and discussion

3.1. Spatial variations in $PBM_{2.5}$ concentration and isotopic composition

The average $PBM_{2.5}$ concentration in the BTH region was 101.8 ± 118.9 pg m^{-3}, with a range of 2.2–642.3 pg m^{-3} (Table S1). Specifically, the mean $PBM_{2.5}$ concentrations at the five sampling sites (ZJK, CPB, CYB, DXB, and TJ) from northwest to southeast in the BTH increased sequentially, which were 24.5 ± 17.1 (n = 61), 104.5 ± 86.8 (n = 47), 105.4 ± 117.8 (n = 58), 140.2 ± 151.3 (n = 44), and 146.4 ± 137.3 pg m^{-3} (n = 60), respectively. ZJK was located in a rural area with little disturbance from human activities and had the lowest mean $PBM_{2.5}$ concentration. It was comparable to the results of other remote or rural sites in China (16.6–84.5 pg m^{-3}, Summarized in Table S2) but higher than in the global background sites (4.6–11.0 pg m^{-3}) [40]. The mean $PBM_{2.5}$ concentrations in CPB, CYB, DXB, and TJ were significantly higher than those reported in other suburban sites in China (30.0–92.4 pg m^{-3}) but lower than those reported in most other large urban sites in China (Shanghai, Jinan, Xiamen, and Ningbo, 174.4–452.0 pg m^{-3}) (Table S2). Compared with other cities in the world, the $PBM_{2.5}$ concentrations of CPB, CYB, DXB, and TJ were significantly higher than the urban $PBM_{2.5}$ level of 6.34 ± 0.89 pg m^{-3} in Texas in the United States but much lower than the urban $PBM_{2.5}$ concentration of 742.1 ± 304.5 pg m^{-3} in Kathmandu in Nepal [24,25].

Compared with other sampling sites, higher $PBM_{2.5}$ concentrations were observed in DXB and TJ, probably because they were located in Beijing industrial area and Tianjin industrial city, respectively. For the coastal sampling site, the $PBM_{2.5}$ concentration at TJ was much higher than that in other coastal and ocean areas (Table S2). Moreover, Fig. S1 summarizes the observed $PBM_{2.5}$ concentrations in the BTH region in conjunction with previous studies, with a mean value of 117.8 ± 73.7 pg m^{-3} and a range of 24.5–271.5 pg m^{-3}. As we can see, in terms of spatial distribution, the concentration of $PBM_{2.5}$ in the BTH region is highest in urban sites, followed by suburban sites, and lowest in rural sites. Anthropogenic emissions and atmospheric Hg transport were possibly responsible for the $PBM_{2.5}$ in the BTH region. The government has taken a series of air improvement measures in recent years, such as using natural gas instead of coal for heating in winter (http://www.gov.cn/gongbao/content/2013/content_2541901.htm). However, in terms of interannual variation, no significant (P = 0.08) decrease in $PBM_{2.5}$ concentration was observed in the BTH region, which may be related to the lack of observed data in earlier years.

In our study, the mean values of $PBM_{2.5}$ isotopes at all sampling sites in the BTH region were negative for $\delta^{202}Hg$, positive for $\Delta^{199}Hg$, and slightly positive for $\Delta^{200}Hg$ (Table S1). Fig. S2 summarizes the values of $\delta^{202}Hg$ and $\Delta^{199}Hg$ of $PBM_{2.5}$ in this study and other sites in China. The $PBM_{2.5}$ in remote/rural areas had the lowest mean value of $\delta^{202}Hg$ and the highest mean values of $\Delta^{199}Hg$, which were − 1.04 ± 0.46‰ and 0.43 ± 0.35‰ (n = 121, 1 SD), ranging from − 2.48‰ to − 0.19‰ and − 0.20–1.27‰, respectively. The average value of $\delta^{202}Hg$ (−0.96 ± 0.59‰, n = 283, 1 SD) in urban/suburban areas was comparable to the value in remote areas ($P > 0.05$), but the average value of $\Delta^{199}Hg$ was close to zero (0.08 ± 0.34‰, n = 304, 1 SD). Furthermore, both the isotopic composition of $\delta^{202}Hg$ and $\Delta^{199}Hg$ in urban/suburban areas varied considerably, ranging from − 3.28–1.07‰ and − 1.13–1.04‰, respectively. The $PBM_{2.5}$ in coastal areas showed the highest ($P < 0.05$) mean value of $\delta^{202}Hg$ (−0.70 ± 0.68‰, n = 124, 1 SD) and the lowest ($P < 0.05$) mean value of $\Delta^{199}Hg$ (−0.20 ± 0.25‰, n = 124, 1 SD), ranging from-3.69–1.10‰ and − 0.79–0.52‰, respectively.

The mean $\delta^{202}Hg$ value of $PBM_{2.5}$ isotopes in ZJK was − 0.42 ± 0.24‰, significantly ($P < 0.05$) lower than the result (−0.84 ± 0.29‰) of Mt.Ailao in remote areas [22]. While the mean $\delta^{199}Hg$ value of $PBM_{2.5}$ isotopes in ZJK (0.69 ± 0.41‰) was comparable ($P > 0.05$) with Mt.Ailao (−0.66 ± 0.32‰) but significantly ($P < 0.05$) higher than the results of other sampling sites in our study and other remote, suburban/urban, and coastal areas in China [22,28,29,38,44,52,66,68]. Interestingly, the ranges of isotopic composition variation of CPB, CYB, DXB, and TJ mostly overlapped. The mean isotope values of $PBM_{2.5}$ in CPB, CYB, DXB, and TJ had no significant ($P > 0.05$) differences, which were − 0.83 ± 0.31‰, − 0.66 ± 0.45‰, − 0.55 ± 0.21‰, and − 0.64 ± 0.39‰ for $\delta^{202}Hg$ and 0.25 ± 0.19‰, 0.16 ± 0.19‰, 0.15 ± 0.20‰, and 0.17 ± 0.26‰ for $\Delta^{199}Hg$ (Table S1), respectively. Moreover, as can be seen from Fig. S2, the values of $\delta^{202}Hg$ and $\Delta^{199}Hg$ of $PBM_{2.5}$ at these four sampling sites were among that in remote, suburban/ urban, and coastal areas in China. This result means that the $PBM_{2.5}$ in these four sampling sites may have come from the same sources or undergone the same atmospheric processes.

3.2. Seasonal variations in $PBM_{2.5}$ concentration and isotopic composition

Seasonal variations in $PBM_{2.5}$ concentration were observed in the BTH region (Fig. 2, Fig. S3). The $PBM_{2.5}$ concentrations in summer were

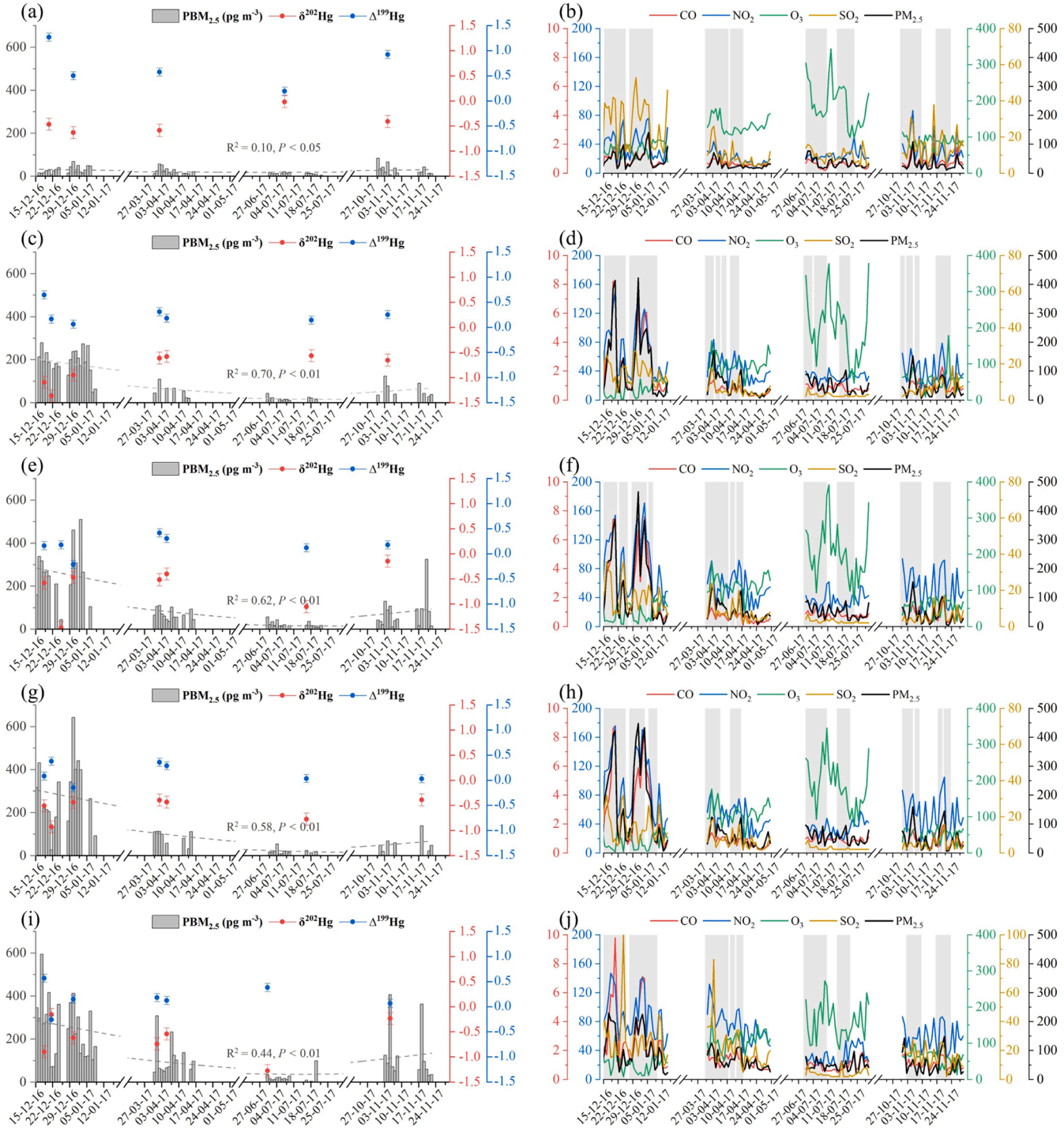

Fig. 2. Daily variations of $PBM_{2.5}$ (pg m^{-3}), $\delta^{202}Hg$ (‰), $\Delta^{199}Hg$ (‰), CO (mg m^{-3}), NO_2 (ug m^{-3}), O_3 (ug m^{-3}), SO_2 (ug m^{-3}), and $PM_{2.5}$ (ug m^{-3}) at ZJK (a and b), CPB (c and d), CYB (e and f), DXB (g and h), and TJ (i and j) during sampling periods (16 Dec to 15 Jan, Apr, Jul, and Nov). The gray shade in the right figures marks the period in which $PBM_{2.5}$ concentrations were measured. Error bars are 2σ analytical uncertainty of $\delta^{202}Hg$ and $\Delta^{199}Hg$. Dashed curves represent the binomial regression of data.

the lowest ($P < 0.05$) at the five sampling sites, and the $PBM_{2.5}$ concentrations at ZJK, CPB, CYB, DXB, and TJ were comparable ($P > 0.05$) (12.50 ± 4.76, 19.83 ± 9.24, 22.22 ± 13.40, 19.71 ± 11.74, and 22.82 ± 24.11 pg m^{-3}, respectively). The $PBM_{2.5}$ concentrations in winter were the highest ($P < 0.05$) at CPB, CYB, DXB, and TJ, which were 182.43 ± 67.92, 264.35 ± 124.50, 282.86 ± 153.70, and 253.40 ± 135.29 pg m^{-3}, respectively. However, there was no significant ($P > 0.05$) difference in the $PBM_{2.5}$ concentrations of ZJK in winter, spring, and autumn. The concentrations of $PBM_{2.5}$ at the five sampling sites, including ZJK, CPB, CYB, DXB, and TJ, increased sequentially in spring and autumn (except in the autumn of DXB).

Similar seasonal variations in $PBM_{2.5}$ concentration were also found in other studies in northern China [60,61,74]. In summer, the southeast monsoon prevails in the BTH region, and the air masses from the ocean enter the inland, causing significant rainfall. The dilution and removal of $PBM_{2.5}$ by rainfall and the clean air masses from the ocean contributed to the lowest $PBM_{2.5}$ content during this period. Moreover, the temperature in summer was the highest in the BTH region (Fig. S4). High

temperatures that are usually accompanied by low surface pressure and elevated planetary boundary layer heights can accelerate atmospheric exchange and mixing, thus diluting the Hg concentration in the air [67]. Notably, the land use types of ZJK, CPB, CYB, DXB, and TJ were different, but they showed similar $PBM_{2.5}$ concentrations in summer, which indicated that in addition to the impact of local anthropogenic emissions, atmospheric transport also played an important role in $PBM_{2.5}$ levels. In winter, apart from the increased direct $PBM_{2.5}$ emissions caused by heating, meteorological conditions were also unfavorable for $PBM_{2.5}$ diffusion and removal (Fig. S4). The air temperature and the height of the boundary layer decreased in winter, which promoted the stability of the atmosphere and made it difficult for $PBM_{2.5}$ to diffuse. Furthermore, the lowest temperature and higher relative humidity may also have affected the gas-particle distribution of atmospheric Hg, which could have promoted the conversion of GEM and GOM to PBM [21,36,45]. The lower the temperature, the easier the adsorption of gaseous Hg to the fine particles [45]. Higher relative humidity not only facilitates the conversion of GEM to GOM through rapid oxidation in the aqueous phase but also contributes to the adsorption of GOM to aerosols to form PBM. In addition, the rare precipitation in winter in the BTH region is not conducive to the removal of $PBM_{2.5}$. It should be noted that the $PBM_{2.5}$ concentration of ZJK in winter was not significantly different from that in autumn and spring. That may have been due to the diffusion of $PBM_{2.5}$ caused by the higher wind speed in ZJK in winter (Fig. S4), while the prevailing northwest monsoon in winter probably led to the transport of $PBM_{2.5}$ from ZJK to Beijing and TJ (discussed in detail in 3.4).

In our study, $PBM_{2.5}$ samples from all seasons in the BTH region showed negative $\delta^{202}Hg$ values (Fig. 2, Fig. S5, and Table S3), indicating significant contributions from anthropogenic emissions, as the $\delta^{202}Hg$ values from direct anthropogenic emissions are usually negative. The $\delta^{202}Hg$ values varied the largest in winter, with a mean value of $-0.76 \pm 0.38‰$ and a range of $-1.47‰$ - $-0.15‰$, which was comparable to that in summer ($-0.74 \pm 0.49‰$, $-1.28‰$ - $-0.02‰$) (Fig. S5). This result suggests that $PBM_{2.5}$ in winter and summer of the BTH region was affected by various sources or transport. However, the variation of $\delta^{202}Hg$ values in $PBM_{2.5}$ samples in spring and autumn was smaller, which indicates that $PBM_{2.5}$ in spring and autumn had similar sources or experienced the same transport process. The mean $\Delta^{199}Hg$ values in $PBM_{2.5}$ samples in winter, spring, summer, and autumn in the BTH region were $0.25 \pm 0.40‰$, $0.30 \pm 0.14‰$, $0.18 \pm 0.13‰$, and $0.29 \pm 0.36‰$, respectively (Fig. S5). Only three winter $PBM_{2.5}$ samples showed negative $\Delta^{199}Hg$ values, which were likely related to biomass burning characterized by the negative $\Delta^{199}Hg$ values [28]. Moreover, the significant positive correlation between $PBM_{2.5}$ concentration and K^+ in this study also supports this conclusion (Fig. S6). The average $\Delta^{200}Hg$ values in $PBM_{2.5}$ samples in the BTH region were slightly higher than zero, which is in line with previous studies [33,52,79]. There was no significant difference ($P > 0.05$) in the mean $\Delta^{200}Hg$ values in spring, summer, autumn, and winter, and the mean $\Delta^{200}Hg$ value in winter was the lowest, which was $0.03 \pm 0.02‰$. The positive shift of $\Delta^{200}Hg$ values were possibly triggered by the atmospheric Hg(0) photochemical oxidation at the top of the troposphere [9,11].

3.3. Anthropogenic sources contributing to atmospheric $PBM_{2.5}$

In our study, the elevated $PBM_{2.5}$ concentrations were significantly ($P < 0.05$) negatively correlated with low $\Delta^{199}Hg$ values (Fig. S7), similar to the $\Delta^{199}Hg$ signatures of anthropogenic emissions [57], indicating that anthropogenic sources contributed significantly as the increase of $PBM_{2.5}$ concentrations in the BTH region. Fig. 3 summarizes potential $PBM_{2.5}$ emission sources, including soil and dust in Beijing and Hebei, limestone, coal, non-ferrous metal, lichen, and forest foliage/-litter in China [10,16,19,28,31,54-57,6,63,69-71,76,81]. These anthropogenic sources are characterized by negative $\delta^{202}Hg$ values for all sources (mean value from $-2.56 \pm 0.64‰$ to $-0.47 \pm 0.47‰$, 1 SD),

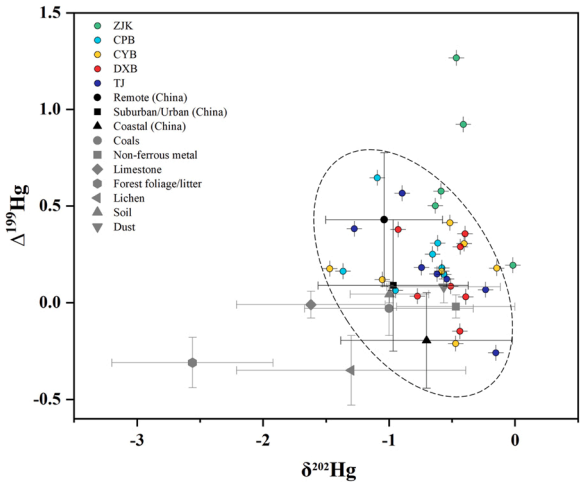

Fig. 3. Hg isotopic compositions of $PBM_{2.5}$ in our study, illustrated with reported data, including soil and dust in Beijing and Hebei, limestone, coal, non-ferrous metal, lichen, and forest foliage/liter in China, and $PBM_{2.5}$ (remote, suburban/urban, and coastal areas) in previous studies.
Source: a) [6,10,16,19,28,31,54,55,56,57,63,69,70,71,76,81], b) [22,28,29,38,44,52,66,68].

negative $\Delta^{199}Hg$ values for lichen and forest foliage/litter (mean values were $-0.35 \pm 0.18‰$ and $-0.31 \pm 0.13‰$, respectively, 1 SD), and near-zero $\Delta^{199}Hg$ values for soil, dust, limestone, coal, and non-ferrous metal (mean values were $0.04 \pm 0.05‰$, $0.08 \pm 0.08‰$, $-0.01 \pm 0.07‰$, $-0.03 \pm 0.14‰$, and $-0.02 \pm 0.06‰$, respectively, 1 SD).

The $\delta^{202}Hg$ values in all $PBM_{2.5}$ samples overlapped with summarized Hg emission sources (Fig. 3), demonstrating that these anthropogenic emission sources significantly contributed to the $PBM_{2.5}$ in the BTH region. However, the majority of the $\Delta^{199}Hg$ values in $PBM_{2.5}$ samples were higher than those in anthropogenic sources, and only some overlapped (Fig. 3). For example, negative $\Delta^{199}Hg$ values were observed at CYB, DXB, and TJ in winter, which was probably from biomass burning [28]. In that regard, [44] have pointed out that biomass burning from northeastern China is one of the main sources of $PBM_{2.5}$ in winter in Beijing. Similar $\Delta^{199}Hg$ values to dust and soil were found in $PBM_{2.5}$ samples at CPB, CYB, DXB, and TJ, which indicates that dust and soil were the sources of $PBM_{2.5}$ in Beijing and Tianjin. Moreover, the $\Delta^{199}Hg$ values of $PBM_{2.5}$ at DXB suggested that it was likely affected by dust, soil, coal, and non-ferrous metal. Considering that many $PBM_{2.5}$ samples showed higher $\Delta^{199}Hg$ values than anthropogenic sources, we analyzed the relationship between $PBM_{2.5}$ concentrations and $\delta^{15}N\text{-}NH_4^+$ and $\delta^{15}N\text{-}NO_3^-$ values in $PM_{2.5}$ from our previous studies [17] to help identify sources (Fig. 4). The result showed that $PBM_{2.5}$ concentrations were significantly ($p < 0.01$) correlated with $\delta^{15}N\text{-}NH_4^+$ and δ^{15} $N\text{-}NO_3^-$ values. The $\delta^{15}N\text{-}NH_4^+$ and $\delta^{15}N\text{-}NO_3^-$ values in $PM_{2.5}$ samples overlapped with those in coal combustion, biomass burning, traffic emissions, and livestock waste [5,34]. In summary, soil, dust, coal combustion, biomass burning, and non-ferrous metal probably were the main anthropogenic sources of $PBM_{2.5}$ in the BTH region.

In addition to isotopic composition analysis, Pearson correlation analysis was performed between $PBM_{2.5}$ and typical air pollutants ($PM_{2.5}$, CO, NO_2, and SO_2) that showed similar seasonal variations (Fig. 2). Except for ZJK, the $PBM_{2.5}$ concentration was significantly ($P < 0.05$) positively correlated with the $PM_{2.5}$ content at CPB, CYB, DXB, and TJ (Fig. S8). Additionally, the $PBM_{2.5}/PM_{2.5}$ slope increased sequentially, making it possible to reveal the direction of the $PBM_{2.5}$ source to a certain extent [77]. The $PBM_{2.5}$ and $PM_{2.5}$ contents in ZJK were the lowest, and no significance was observed between them, which probably was related to the low human activities in ZJK and the transport of dust with low Hg concentration from Inner Mongolia. However, anthropogenic sources contributed more to the atmospheric higher Hg

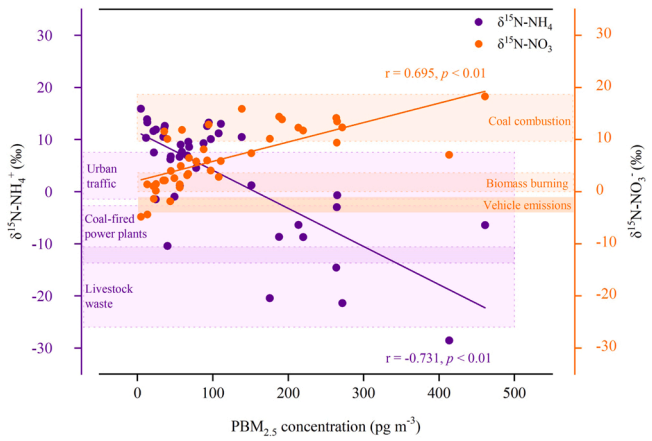

Fig. 4. Relationship between $\delta^{15}N\text{-}NH_4^+$ and $\delta^{15}N\text{-}NO_3^-$ in $PM_{2.5}$ and $PBM_{2.5}$ concentrations in the BTH region in this study. Data of $\delta^{15}N\text{-}NH_4^+$ and $\delta^{15}N\text{-}NO_3^-$ were taken from our previous study. Purple and orange shades indicate the source signatures of $\delta^{15}N\text{-}NH_4^+$ and $\delta^{15}N\text{-}NO_3^-$ overviewed by previous studies. Source: [5,17,34].

particles at CPB, CYB, DXB, and TJ because of the sequentially increased land-use intensity. The $PBM_{2.5}/PM_{2.5}$ slope in TJ was the highest. In addition to the difference in anthropogenic emissions, it may also be that TJ had the highest atmospheric relative humidity ($P < 0.01$), which can promote gas-particle partitioning, facilitating the conversion of other forms of Hg to PBM [20,43,75]. Furthermore, the $PBM_{2.5}$ concentrations at the five sampling sites were significantly correlated with CO, SO_2, and NO_2 concentrations (Table S4), suggesting that fossil fuel combustion was an important source of $PBM_{2.5}$. Besides ZJK, the $PBM_{2.5}$ concentrations of other sites were significantly correlated with each other, suggesting that they may have come from the same sources (Table S4).

In our study, regression analyses were also employed to analyze the relationship between $PBM_{2.5}$ and the anions/cations concentrations in $PM_{2.5}$ (Fig. S6). Specifically, the $PBM_{2.5}$ in Beijing and Tianjin was significantly positively correlated with Na^+ in $PM_{2.5}$, mainly from sea-salt [17]. The $PBM_{2.5}$ at all sampling sites was significantly positively related to Mg^{2+} in $PM_{2.5}$, especially at ZJK ($r = 0.86$, $p < 0.01$), and Mg^{2+} in $PM_{2.5}$ mainly came from dust/soil [62], which showed that dust/soil contributed greatly to the $PBM_{2.5}$ of ZJK. The $PBM_{2.5}$ in the BTH region was also significantly positively correlated with K^+, NH_4^+, and NO_3^- in $PM_{2.5}$ (Fig. S6), indicating that the contribution of biomass burning (also supported by fire maps, Fig. S9) to $PBM_{2.5}$ could not be ignored. Moreover, the $PBM_{2.5}$ in Beijing and Tianjin were significantly correlated with Cl^- and SO_4^{2-} in $PM_{2.5}$, mainly derived from fossil fuel combustion [62], suggesting that fossil fuel combustion was a significant source of $PBM_{2.5}$. In addition, SO_4^{2-} and NO_3^- can also affect the gas-particle partitioning of atmospheric Hg. The contents of SO_4^{2-} and NO_3^- accounted for 15.2 ± 8.5% and 11.4 ± 5.7% of $PM_{2.5}$ in the BTH region, respectively. Rutter et al. [46] reported that NO_3^- had a high partitioning coefficient, which can convert GOM partitioning to PBM. Chen et al. [13] pointed out that SO_4^{2-} was facilitated to form $HgSO_4$, $HgSO_3$, and HgS from GEM and adsorbed on PM. The anthropogenic sources identified by the relationship between $PBM_{2.5}$ and atmospheric environmental factors well supported the results of isotopic sources analysis. It shows that the combination of Hg isotopes and nitrogen isotopes is more conducive to accurately identifying the anthropogenic emission source. Principle component analysis - multiple linear regression (PCA-MLR) was employed to quantify the contributions of different sources to $PBM_{2.5}$ in the BTH region (Text S3). PCA results showed that four principal factors accounting for 80.2% of the total variance were extracted, which represented combustion, sea-salt, atmospheric process, and dust/soil contributions, respectively (Table S5). MLR results ($R^2 = 0.808$, $P < 0.01$) indicated that these four factors contributed 47.9%, 20.2%, 17.0%, and 14.9% of $PBM_{2.5}$, respectively, i.e., the contribution of anthropogenic sources was 62.8% and that of the natural sources was 37.2%.

3.4. Long-range transboundary transport contributing to $PBM_{2.5}$

Fig. 3 also summarizes the $\delta^{202}Hg$ and $\Delta^{199}Hg$ values of $PBM_{2.5}$ in the remote (−1.04 ± 0.46‰ for $\delta^{202}Hg$, 0.43 ± 0.35‰ for $\Delta^{199}Hg$, n = 121, 1 SD) suburban/urban (−0.97 ± 0.60‰ for $\delta^{202}Hg$, −0.09 ± 0.34‰ for $\Delta^{199}Hg$, n = 297, 1 SD), and coastal areas (−0.70 ± 0.68‰ for $\delta^{202}Hg$, −0.20 ± 0.25‰ for $\Delta^{199}Hg$, n = 124, 1 SD) in China [22,28,29,38,44,52,66,68]. The $\delta^{202}Hg$ values of $PBM_{2.5}$ in the BTH region overlapped with the $\delta^{202}Hg$ values of anthropogenic sources and that of $PBM_{2.5}$ in other areas (Fig. 3). However, the majority of $\Delta^{199}Hg$ values in the BTH were higher than the $\Delta^{199}Hg$ values of anthropogenic sources but overlapped with the $\Delta^{199}Hg$ values of $PBM_{2.5}$ in other areas, including remote, suburban/urban, and coastal areas. This result reveals that the atmospheric transport processes were more likely to directly contribute to the $PBM_{2.5}$ isotopic variations in the BTH region, especially the higher $\Delta^{199}Hg$ of $PBM_{2.5}$ in all sites overlapped with that in remote sites (Fig. 3). The long-range transport of $PBM_{2.5}$ emitted by anthropogenic sources through the middle and low free troposphere leads to a positive shift of $\Delta^{199}Hg$ of $PBM_{2.5}$ under strong photoreduction [44]. Moreover, the photochemical reduction of anthropogenic $PBM_{2.5}$ during long-distance transport also shows decreased $PBM_{2.5}$ concentrations in addition to increased $\Delta^{199}Hg$ values [22]. Photoreduction of divalent mercury ion (Hg(II)) preferentially inhibits the odd-MIF of Hg isotopes in the reactant (here $PBM_{2.5}$), resulting in a positive shift of $\Delta^{199}Hg$ [4]. The ratio of $\Delta^{199}Hg/\Delta^{201}Hg$ is widely used to identify changes in the MIF of Hg isotopes of $PBM_{2.5}$ during transport in the atmosphere before collection [51,66,68,73]. In our study, $\Delta^{199}Hg$ and $\Delta^{201}Hg$ values of $PBM_{2.5}$ were significantly positively correlated (Fig. 5), and the slope closed to the ratio of $\Delta^{199}Hg/\Delta^{201}Hg$ (1.00–1.31) resulting from the photoreduction of inorganic Hg(II) with dissolved organic carbon in sulfur-free aqueous solutions [4,80]. The photoreduction of Hg(II) induces positive odd-MIF in residual Hg(II), contributing to the positive $\Delta^{199}Hg$ of $PBM_{2.5}$ observed in the BTH region.

The East Asian monsoon significantly impacted the transport of air masses reaching the BTH region. In winter, the air masses from the west and northwest mainly traveled through Central Asia, Russian Siberia, and Mongolia for long-distance transport to the sampling sites (Fig. S10). The transport height of these air masses was between 900 kPa - 500kPa, mainly above the planetary boundary layer and in the middle and lower troposphere. The long-distance transport in the atmospheric troposphere can lead to the strong photoreduction of $PBM_{2.5}$, which promotes the positive shift of $\Delta^{199}Hg$ [12,44]. This result also supports the higher $\Delta^{199}Hg$ values in winter observed in this study (Fig. 2, Fig. S5). In summer, the transport of mid-distance and short-distance air masses was dominant (Fig. S10). In ZJK, the air mass (<900 kPa) from the southeast had the greatest influence in ZJK, which was 39.46%. In Beijing (CPB, CYB, and DXB), the regional air mass transport around the BTH region was also impacted significantly in addition to the air mass from southeast China. In TJ, more than 60% of the air mass came from the ocean and southeastern China. Generally, these air masses from the southeast carrying low Hg levels and more rainfall are an important reason for the low summer $PBM_{2.5}$ content in the BTH region. Moreover, the transport of these air masses showed low heights and shorter distances, indicating that the $\Delta^{199}Hg$ of $PBM_{2.5}$ in the BTH region was weakly affected by the atmospheric photoreduction in summer [22]. In spring and autumn, the air masses from the northwest mainly passed through Kazakhstan, Russia, Mongolia, and Inner Mongolia for long-distance transport to the sampling sites. It should be noted that the impact of air masses from western China on ZJK cannot be ignored. But the presence of the Yanshan and Taihang Mountains may have prevented the further transport of these low-altitude air masses to Beijing and Tianjin.

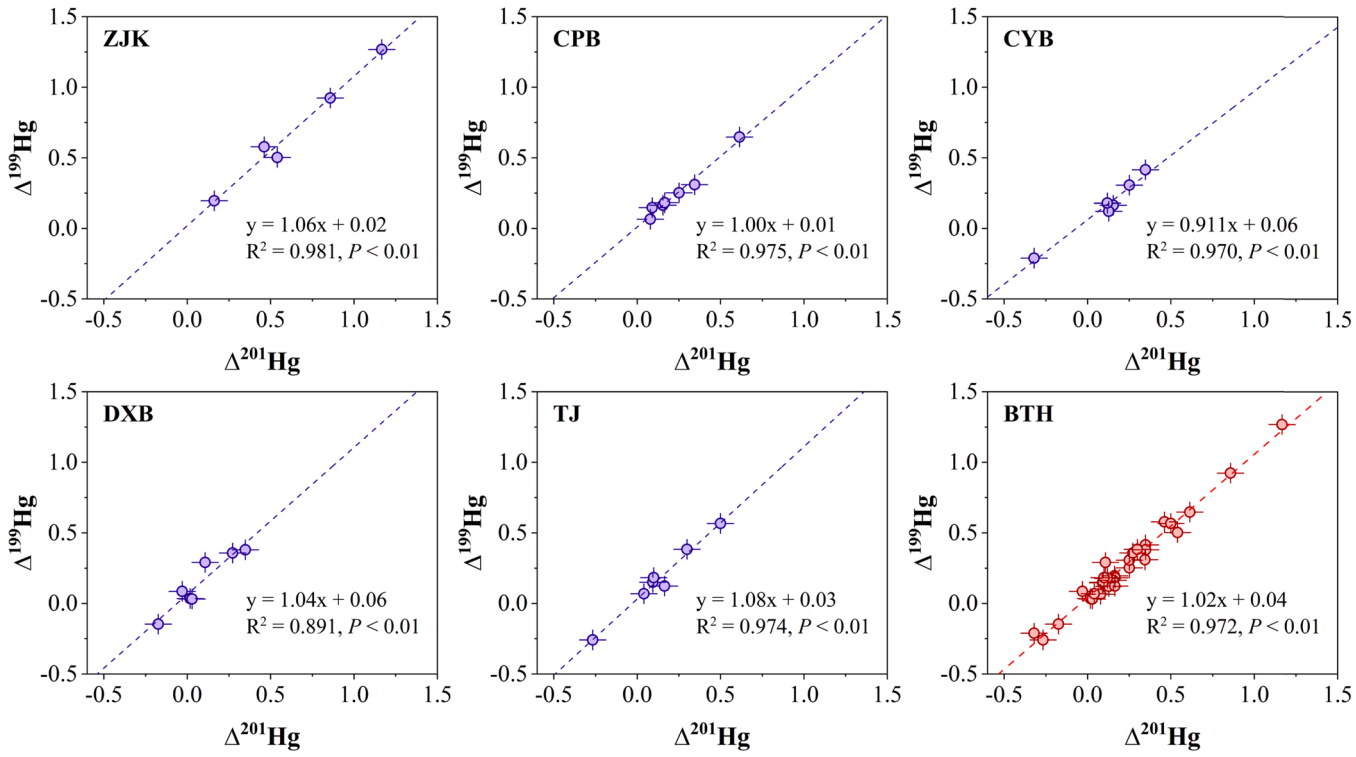

Fig. 5. Line regressions of $\Delta^{199}Hg/\Delta^{201}Hg$ of $PBM_{2.5}$ at the five sampling sites in the BTH region.

PSCF is employed to identify potential source regions of $PBM_{2.5}$ in the BTH region, with a criterion set at 24.5 pg m^{-3}, the average $PBM_{2.5}$ concentration of ZJK. $PBM_{2.5}$ concentrations above and below 24.5 pg m^{-3} are considered as potential pollution sources (Fig. 6) and clean sources (Fig. 7), respectively. The potential pollution source regions of $PBM_{2.5}$ in the BTH region were associated with the transport of air masses from the west and northwest (Fig. 6, Fig. S10). For instance, the potential pollution source regions of the $PBM_{2.5}$ of ZJK were located in southeastern Mongolia, Inner Mongolia, northern Shaanxi, and northern Shanxi. The potential pollution sources of $PBM_{2.5}$ in CPB, CYB, DXB, and TJ were located in Mongolia, Inner Mongolia, and regional emissions of BTH. In addition, the southern provinces of BTH, including Shandong, Henan, Anhui, and Jiangsu, were also potential pollution source regions of $PBM_{2.5}$ in TJ. Interestingly, crossing from northwest to southeast along the BTH region, the emissions from the southern province of BTH also showed increasing impacts on the $PBM_{2.5}$ of the BTH region. It suggests that the contribution of the East Asian monsoon to atmospheric $PBM_{2.5}$ in southeastern China and the oceanic may be more significant as the East Asian monsoon passes through the heavily polluted eastern China.

As shown in Fig. 1a, the BTH region and its surrounding areas were the large sources of anthropogenic Hg emissions in China [1], which contributed significantly to the $PBM_{2.5}$ concentrations in the BTH region. Although the atmospheric Hg emissions in Mongolia were low, the transport of Hg from Central Asia and Russia along the East Asian monsoon could also significantly impact the $PBM_{2.5}$ in the BTH region (Fig. 1a, Fig. S10). It should be noted that these air masses reaching the BTH region would carry elevated $PBM_{2.5}$ concentrations further transported to the ocean by the East Asian monsoon. In addition, the dust and sand transported to the BTH region under the influence of the northwest monsoon provided a medium for the adsorption of atmospheric Hg, further increasing the atmospheric $PBM_{2.5}$ content [74].

The potential clean source regions with $PBM_{2.5}$ concentrations less than 24.5 pg m^{-3} were mainly from the southeast of BTH except for ZJK, which was related to the air masses from the southeast of the ocean in summer (Fig. 7, Fig. S10). The clean air mass transported by the southeast monsoon from the Yellow Sea and the Bohai Sea contributed significantly to the low $PBM_{2.5}$ concentration in the BTH region (Fig. 7). In addition to the clean air masses from the southeasterly wind, the dilution of clean sources from Inner Mongolia and Mongolia also significantly affected the $PBM_{2.5}$ concentrations at ZJK. However, Yanshan and Taihang Mountains may have prevented these low-altitude clean air masses from being further transported to the southeast, or these clean air masses may have become polluted air masses with increased $PBM_{2.5}$ during transport. Overall, the southeast air masses from the ocean driven by the East Asian monsoon have a scavenging effect on the inland atmospheric $PBM_{2.5}$, especially in the coastal areas.

$PBM_{2.5}$ from anthropogenic emissions typically exhibits negative $\delta^{202}Hg$ and near-zero or negative $\Delta^{199}Hg$, whereas $PBM_{2.5}$ from background pools showed negative $\delta^{202}Hg$ and positive $\Delta^{199}Hg$ (Fig. 3). The MDF of $\delta^{202}Hg$ is unstable and easily affected by physicochemical reactions, while the odd-MIF $\Delta^{199}Hg$ is only triggered by photochemical reactions. Therefore, the backward trajectory combined with $\Delta^{199}Hg$ is used to identify the potential sources of regional transport [72,73]. We assumed that the $\Delta^{199}Hg$ values of $PBM_{2.5}$ above the average value of the BTH region (0.26‰, significantly higher than anthropogenic sources shown in Fig. 3) were from clean background sources, while those below the mean value were from anthropogenic emissions (Fig. S11). The trajectories with high $\Delta^{199}Hg$ values mainly originated in southwestern Kazakhstan, southern Siberia, the coastal cities in southeastern China, and the Yellow Sea. In contrast, the trajectories with low $\Delta^{199}Hg$ values originated in western and southwestern Siberia, eastern Kazakhstan, and inland cities in southern China. These supported the result of the potential source regions of $PBM_{2.5}$ in the BTH region determined by the backward trajectories and $PBM_{2.5}$ concentrations.

4. Conclusions

Our study found that different landforms and anthropogenic activities had significant effects on atmospheric $PBM_{2.5}$ emissions. Combining Hg and nitrogen stable isotopes can help accurately identify atmospheric Hg sources. Anthropogenic emissions such as coal

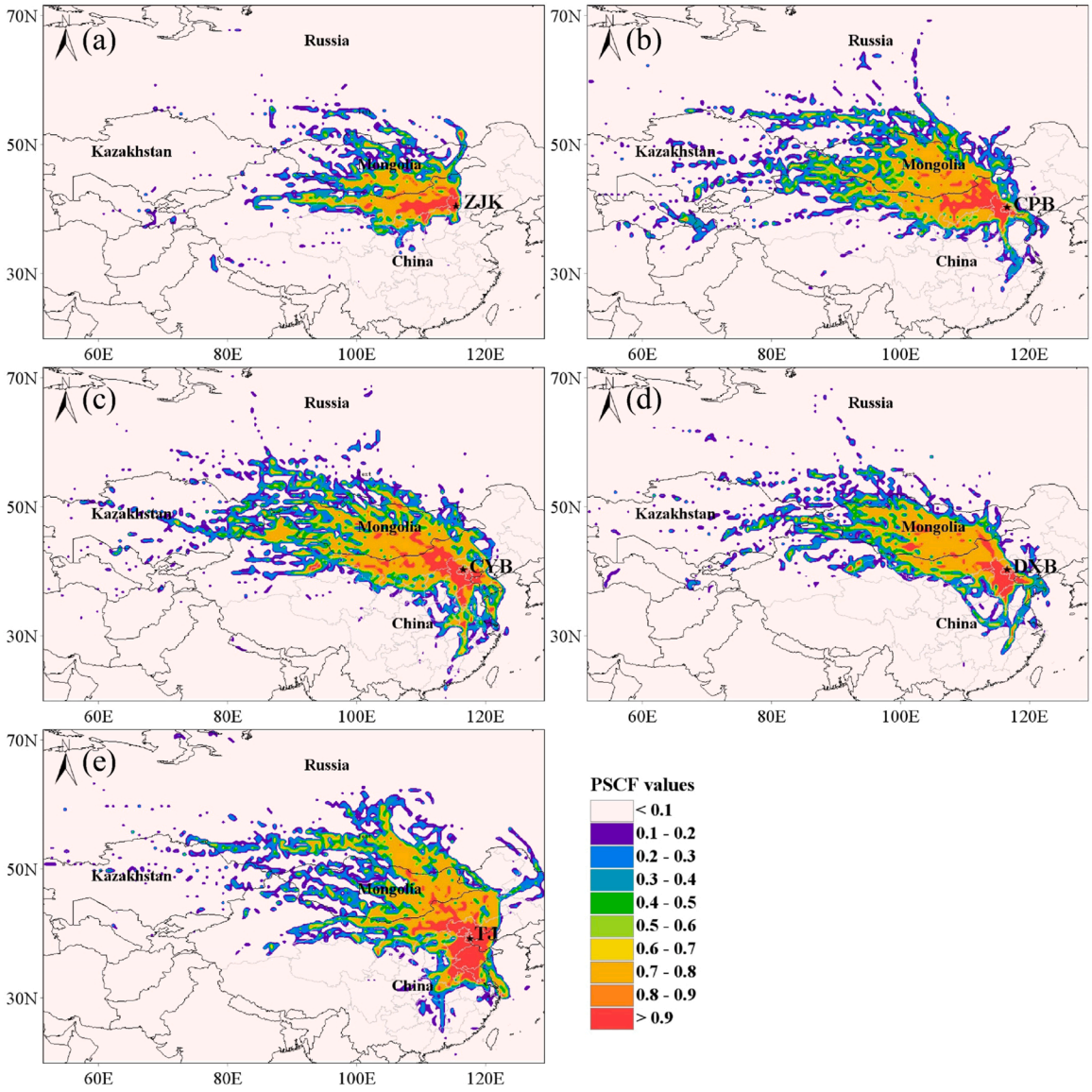

Fig. 6. Potential pollution source regions associated with elevated atmospheric $PBM_{2.5}$ concentrations (>24.5 pg m^{-3}) at ZJK (a), CPB (b), CYB (c), DXB (d), and TJ (e).

combustion, non-ferrous metal, and soil/dust were the primary sources of $PBM_{2.5}$ in the BTH region based on the isotope and PCA-MLR analyses. The positive Δ^{199}Hg values and high concentrations of $PBM_{2.5}$ also indicated that in addition to the regional anthropogenic $PBM_{2.5}$ emissions, the Hg transport, driven by the East Asian monsoon, contributed significantly to the atmospheric $PBM_{2.5}$. Affected by the air masses from the northwest and west (originating in Russia and Central Asia, respectively), the potential pollution sources of $PBM_{2.5}$ in the BTH region were mainly located in Mongolia and Inner Mongolia. These air masses reaching the BTH region would carry elevated $PBM_{2.5}$ concentrations further transported to the ocean by the East Asian monsoon. By contrast, the clean air mass transported by the southeast monsoon from the ocean in summer diluted the atmospheric $PBM_{2.5}$ pollution, especially in the coastal areas. The atmospheric $PBM_{2.5}$ underwent intense photoreduction under the long-distance transport driven by the East Asian monsoon, resulting in elevated Δ^{199}Hg values of $PBM_{2.5}$. It suggests that photoreduction is the predominant reaction during atmospheric PBM transport, reflecting the usefulness of Hg isotopes in tracing atmospheric Hg transport and conversion processes. In addition, long-range transport not only increases the Hg content in the arriving areas but also leads to Hg reemission from rapidly deposited PBM by photoreduction during transport, thus extending the life and diffusion of Hg. Our study provides clear evidence for the transport, transformation, and circulation of atmospheric $PBM_{2.5}$ by using Hg isotopes.

CRediT authorship contribution statement

Xuechao Qin: Conceptualization, Methodology, Software, Formal analysis, Writing – original draft, Writing – review & editing. **Xinyuan Dong**: Methodology, Formal analysis. **Zhenghua Tao**: Software, Investigation. **Rongfei Wei**: Investigation. **Hua Zhang**: Validation, Resources. **Qingjun Guo**: Conceptualization, Validation, Supervision, Writing – review & editing.

Declaration of Competing Interest

The authors declare that they have no known competing financial interests or personal relationships that could have appeared to influence the work reported in this paper.

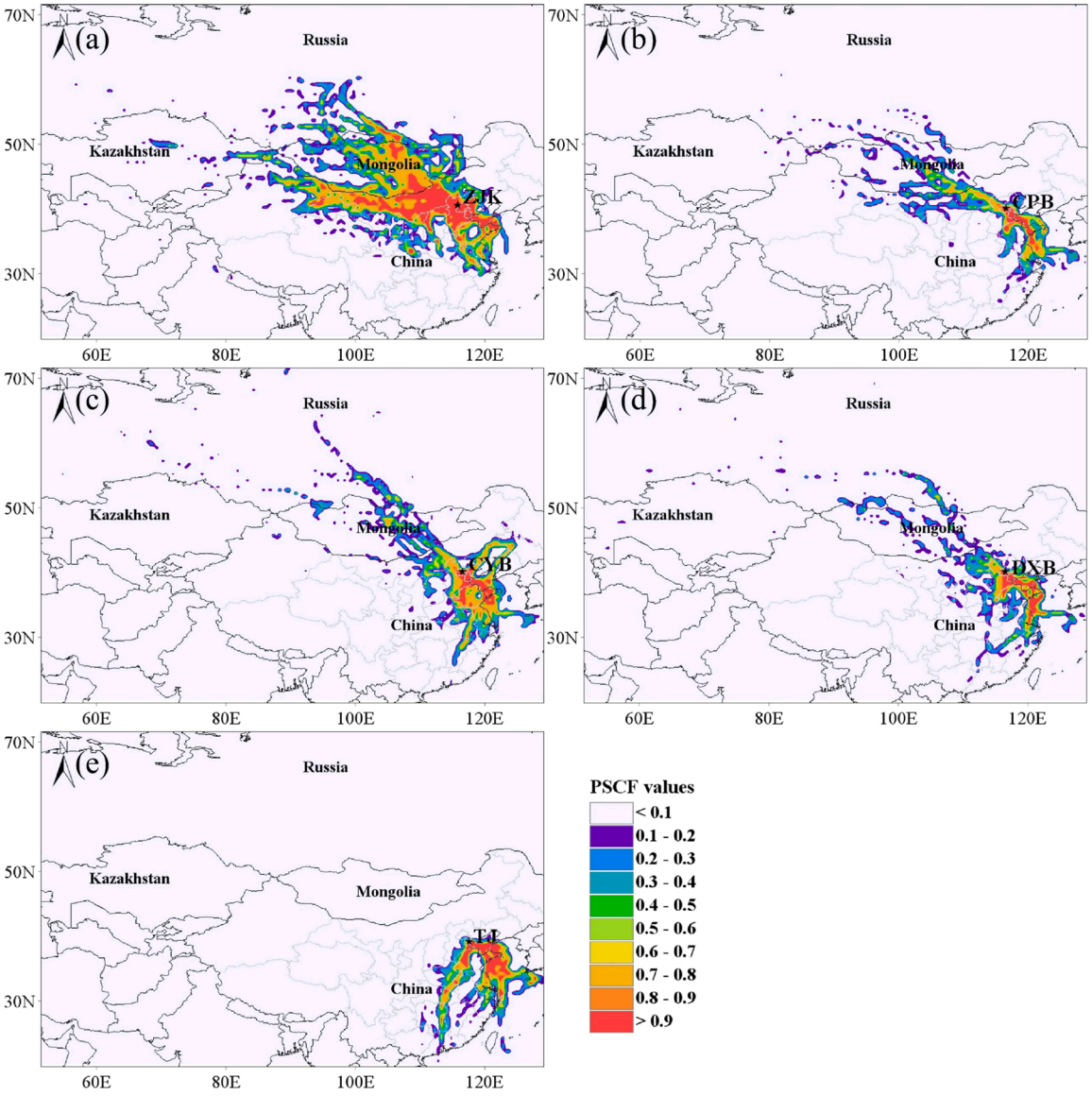

Fig. 7. Potential clean source regions associated with low atmospheric $PBM_{2.5}$ concentrations (<24.5 pg m^{-3}) at ZJK (a), CPB (b), CYB (c), DXB (d), and TJ (e).

Data Availability

Data will be made available on request.

Acknowledgments

This study was supported by National Key Research and Development Program of China (No. 2017YFC0212703), National Natural Science Foundation of China (Grant Nos. 41625006, 41761144066, 41561144005, 41890824, 41890822), and Cross-Team and Key Laboratory Cooperative Research Special Project of Chinese Academy of Sciences (CAS "Light of West China" Program).

Appendix A. Supporting information

Supplementary data associated with this article can be found in the online version at doi:10.1016/j.jhazmat.2022.130678.

References

[1] AMAP/UNEP (2019). Technical Background Report to the Global Mercury Assessment 2018, Arctic Monitoring and Assessment Programme, Oslo. Norway/UNEP, Chemicals and Health Branch, Geneva, Switzerland.
[2] Amos, H.M., Jacob, D.J., Holmes, C.D., Fisher, J.A., Wang, Q., Yantosca, R.M., et al., 2012. Gas-particle partitioning of atmospheric Hg(II) and its effect on global mercury deposition. Atmos Chem Phys 12 (1), 591–603. https://doi.org/10.5194/acp-12-591-2012.
[3] Ariya, P.A., Amyot, M., Dastoor, A., Deeds, D., Feinberg, A., Kos, G., et al., 2015. Mercury physicochemical and biogeochemical transformation in the atmosphere and at atmospheric interfaces: a review and future directions. Chem Rev 115 (10), 3760–3802. https://doi.org/10.1021/cr500667e.
[4] Bergquist, B.A., Blum, J.D., 2007. Mass-dependent and -independent fractionation of Hg isotopes by photoreduction in aquatic systems. Science 318, 417–420.
[5] Bhattarai, N., Wang, S., Pan, Y., Xu, Q., Zhang, Y., Chang, Y., et al., 2021. delta(15) N-stable isotope analysis of NH x: an overview on analytical measurements, source sampling and its source apportionment. Front Environ Sci Eng 15 (6), 126. https://doi.org/10.1007/s11783-021-1414-6.
[6] Biswas, A., Blum, J.D., Bergquist, B.A., Keeler, G.J., Xie, Z., 2008. Natural mercury isotope variation in coal deposits and organic soils. Environ Sci Technol 42 (22), 8303–8309. https://doi.org/10.1021/es801444b.
[7] Blum, J.D., Bergquist, B.A., 2007. Reporting of variations in the natural isotopic composition of mercury. Anal Bioanal Chem 388 (2), 353–359. https://doi.org/10.1007/s00216-007-1236-9.

[8] Blum, J.D., Sherman, L.S., Johnson, M.W., 2014. Mercury isotopes in earth and environmental sciences. Annu Rev Earth Planet Sci 42 (1), 249–269. https://doi.org/10.1146/annurev-earth-050212-124107.
[9] Cai, H., Chen, J., 2016. Mass-independent fractionation of even mercury isotopes. Sci Bull 61 (2), 116–124. https://doi.org/10.1007/s11434-015-0968-8.
[10] Carignan, J., Estrade, N., Sonke, J.E., Donard, O.F.X., 2009. Odd isotope deficits in atmospheric Hg measured in lichens. Environ Sci Technol 43 (15), 5660–5664. https://doi.org/10.1021/es900578v.
[11] Chen, J., Hintelmann, H., Feng, X., Dimock, B., 2012. Unusual fractionation of both odd and even mercury isotopes in precipitation from Peterborough, ON, Canada. Geochim Et Cosmochim Acta 90, 33–46. https://doi.org/10.1016/j.gca.2012.05.005.
[12] Chen, J.B., Hintelmann, H., Feng, X.B., Dimock, B., 2012. Unusual fractionation of both odd and even mercury isotopes in precipitation from Peterborough, ON, Canada. Geochim Et Cosmochim Acta 90, 33–46. https://doi.org/10.1016/j.gca.2012.05.005.
[13] Chen, X.J., Balasubramanian, R., Zhu, Q.Y., Behera, S.N., Bo, D.D., Huang, X., et al., 2016. Characteristics of atmospheric particulate mercury in size-fractionated particles during haze days in Shanghai. Atmos Environ 131, 400–408. https://doi.org/10.1016/j.atmosenv.2016.02.019.
[14] Chen, Z., Chen, D., Zhao, C., Kwan, M.P., Cai, J., Zhuang, Y., et al., 2020. Influence of meteorological conditions on PM2.5 concentrations across China: a review of methodology and mechanism. Environ Int 139 (105558). https://doi.org/10.1016/j.envint.2020.105558.
[15] Cheng, I., Xu, X., Zhang, L., 2015. Overview of receptor-based source apportionment studies for speciated atmospheric mercury. Atmos Chem Phys 15 (14), 7877–7895. https://doi.org/10.5194/acp-15-7877-2015.
[16] Demers, J.D., Blum, J.D., Zak, D.R., 2013. Mercury isotopes in a forested ecosystem: Implications for air-surface exchange dynamics and the global mercury cycle. Glob Biogeochem Cycles 27 (1), 222–238. https://doi.org/10.1002/gbc.20021.
[17] Dong, X., Guo, Q., Han, X., Wei, R., Tao, Z., 2022. The isotopic patterns and source apportionment of nitrate and ammonium in atmospheric aerosol. Sci Total Environ 803, 149559. https://doi.org/10.1016/j.scitotenv.2021.149559.
[18] Driscoll, C.T., Mason, R.P., Chan, H.M., Jacob, D.J., Pirrone, N., 2013. Mercury as a global pollutant: sources, pathways, and effects. Environ Sci Technol 47 (10), 4967–4983. https://doi.org/10.1021/es305071v.
[19] Enrico, M., Le Roux, G., Marusczak, N., Heimburger, L.E., Claustres, A., Fu, X.W., et al., 2016. Atmospheric mercury transfer to peat bogs dominated by gaseous elemental mercury dry deposition. Environ Sci Technol 50 (5), 2405–2412. https://doi.org/10.1021/acs.est.5b06058.
[20] Fain, X., Obrist, D., Hallar, A.G., McCubbin, I., Rahn, T., 2009. High levels of reactive gaseous mercury observed at a high elevation research laboratory in the rocky mountains. Atmos Chem Phys 9 (20), 8049–8060. https://doi.org/10.5194/acp-9-8049-2009.
[21] Faïn, X., Obrist, D., Hallar, A.G., McCubbin, I., Rahn, T., 2009. High levels of reactive gaseous mercury observed at a high elevation research laboratory in the rocky mountains. Atmos Chem Phys 9 (20), 8049–8060. https://doi.org/10.5194/acp-9-8049-2009.
[22] Fu, X., Zhang, H., Feng, X., Tan, Q., Ming, L., Liu, C., et al., 2019. Domestic and transboundary sources of atmospheric particulate bound mercury in remote areas of china: evidence from mercury isotopes. Environ Sci Technol 53 (4), 1947–1957. https://doi.org/10.1021/acs.est.8b06736.
[23] Gratz, L.E., Keeler, G.J., Blum, J.D., Sherman, L.S., 2010. Isotopic composition and fractionation of mercury in great lakes precipitation and ambient air. Environ Sci Technol 44 (20), 7764–7770. https://doi.org/10.1021/es100383w.
[24] Griggs, T., Liu, L., Talbot, R.W., Torres, A., Lan, X., 2020. Comparison of atmospheric mercury speciation at a coastal and an urban site in Southeastern Texas, USA. Atmosphere 11 (1), 73. https://doi.org/10.3390/atmos11010073.
[25] Guo, J.M., Sharma, C.M., Tripathee, L., Kang, S.C., Fu, X.W., Huang, J., et al., 2021. Source identification of atmospheric particle-bound mercury in the Himalayan foothills through non-isotopic and isotope analyses. Environ Pollut 286, 117317. https://doi.org/10.1016/j.envpol.2021.117317.
[26] Hintelmann, H., Lu, S., 2003. High precision isotope ratio measurements of mercury isotopes in cinnabar ores using multi-collector inductively coupled plasma mass spectrometry. Analyst 128 (6), 635–639. https://doi.org/10.1039/b300451a.
[27] Horowitz, H.M., Jacob, D.J., Zhang, Y.X., Dibble, T.S., Slemr, F., Amos, H.M., et al., 2017. A new mechanism for atmospheric mercury redox chemistry: implications for the global mercury budget. Atmos Chem Phys 17 (10), 6353–6371. https://doi.org/10.5194/acp-17-6353-2017.
[28] Huang, Q., Chen, J.B., Huang, W.L., Fu, P.Q., Guinot, B., Feng, X.B., et al., 2016. Isotopic composition for source identification of mercury in atmospheric fine particles. Atmos Chem Phys 16 (18), 11773–11786. https://doi.org/10.5194/acp-16-11773-2016.
[29] Huang, Q., Chen, J.B., Huang, W.L., Reinfelder, J.R., Fu, P.Q., Yuan, S.L., et al., 2019. Diel variation in mercury stable isotope ratios records photoreduction of PM2.5-bound mercury. Atmos Chem Phys 19 (1), 315–325. https://doi.org/10.5194/acp-19-315-2019.
[30] Huang, Q., Liu, Y.L., Chen, J.B., Feng, X.B., Huang, W.L., Yuan, S.L., et al., 2015. An improved dual-stage protocol to pre-concentrate mercury from airborne particles for precise isotopic measurement. J Anal At Spectrom 30 (4), 957–966. https://doi.org/10.1039/c4ja00438h.
[31] Jiskra, M., Wiederhold, J.G., Skyllberg, U., Kronberg, R.-M., Hajdas, I., Kretzschmar, R., 2015. Mercury deposition and re-emission pathways in boreal forest soils investigated with Hg isotope signatures. Environ Sci Technol 49 (12), 7188–7196. https://doi.org/10.1021/acs.est.5b00742.
[32] Jonsson, S., Skyllberg, U., Nilsson, M.B., Lundberg, E., Andersson, A., Bjorn, E., 2014. Differentiated availability of geochemical mercury pools controls methylmercury levels in estuarine sediment and biota. Nat Commun 5, 4624. https://doi.org/10.1038/ncomms5624.
[33] Li, C.J., Chen, J.B., Angot, H., Zheng, W., Shi, G.T., Ding, M.H., et al., 2020. Seasonal variation of mercury and its isotopes in atmospheric particles at the Coastal Zhongshan Station, Eastern Antarctica. Environ Sci Technol 54 (18), 11344–11355. https://doi.org/10.1021/acs.est.0c04462.
[34] Li, Z., Walters, W.W., Hastings, M.G., Zhang, Y., Song, L., Liu, D., et al., 2019. Nitrate isotopic composition in precipitation at a Chinese megacity: seasonal variations, atmospheric processes, and implications for sources. Earth Space Sci 6 (11), 2200–2213. https://doi.org/10.1029/2019ea000759.
[35] Li, Z.G., Chen, X.F., Liu, W.L., Li, T.S., Chen, J., Lin, C.J., et al., 2019. Evolution of four-decade atmospheric mercury release from a coal-fired power plant in North China. Atmos. Environ. 213, 526–533. https://doi.org/10.1016/j.atmosenv.2019.06.045.
[36] Lin, H.M., Tong, Y.D., Yin, X.F., Zhang, Q.G., Zhang, H., Zhang, H.R., et al., 2019. First measurement of atmospheric mercury species in Qomolangma Natural Nature Preserve, Tibetan Plateau, and evidence of transboundary pollutant invasion. Atmos Chem Phys 19 (2), 1373–1391. https://doi.org/10.5194/acp-19-1373-2019.
[37] Lindberg, S., Bullock, R., Ebinghaus, R., Engstrom, D., Feng, X.B., Fitzgerald, W., et al., 2007. A synthesis of progress and uncertainties in attributing the sources of mercury in deposition. Ambio 36 (1), 19–32. https://doi.org/10.1579/0044-7447(2007)36[19:Asopau]2.0.Co;2.
[38] Liu, C., Fu, X., Xu, Y., Zhang, H., Wu, X., Sommar, J., et al., 2022. Sources and transformation mechanisms of atmospheric particulate bound mercury revealed by mercury stable isotopes. Environ Sci Technol 56 (8), 5224–5233. https://doi.org/10.1021/acs.est.1c08065.
[39] Lu, X., Zhao, J., Liang, X., Zhang, L., Liu, Y., Yin, X., et al., 2019. The application and potential artifacts of zeeman cold vapor atomic absorption spectrometry in mercury stable isotope analysis. Environ Sci Technol Lett 6 (3), 165–170. https://doi.org/10.1021/acs.estlett.9b00067.
[40] Mao, H., Cheng, I., Zhang, L., 2016. Current understanding of the driving mechanisms for spatiotemporal variations of atmospheric speciated mercury: a review. Atmos Chem Phys 16 (20), 12897–12924. https://doi.org/10.5194/acp-16-12897-2016.
[41] Obrist, D., Tas, E., Peleg, M., Matveev, V., Fain, X., Asaf, D., et al., 2011. Bromine-induced oxidation of mercury in the mid-latitude atmosphere. Nat Geosci 4 (1), 22–26. https://doi.org/10.1038/ngeo1018.
[42] Polissar, A.V., Hopke, P.K., Harris, J.M., 2001. Source regions for atmospheric aerosol measured at Barrow, Alaska. Environ Sci Technol 35 (21), 4214–4226. https://doi.org/10.1021/es0107529.
[43] Qin, X.F., Wang, X.H., Shi, Y.J., Yu, G.Y., Zhao, N., Lin, Y.F., et al., 2019. Characteristics of atmospheric mercury in a suburban area of east China: sources, formation mechanisms, and regional transport. Atmos Chem Phys 19 (9), 5923–5940. https://doi.org/10.5194/acp-19-5923-2019.
[44] Qiu, Y., Gai, P.X., Yue, F.E., Zhang, Y.Y., He, P.Z., Kang, H., et al., 2021. Identification of potential sources of elevated PM2.5-Hg using mercury isotopes during haze events. Atmos Environ 247 (118203). https://doi.org/10.1016/j.atmosenv.2021.118203.
[45] Rutter, A.P., Schauer, J.J., 2007. The effect of temperature on the gas–particle partitioning of reactive mercury in atmospheric aerosols. Atmos Environ 41 (38), 8647–8657. https://doi.org/10.1016/j.atmosenv.2007.07.024.
[46] Rutter, A.P., Schauer, J.J., 2007. The impact of aerosol composition on the particle to gas partitioning of reactive mercury. Environ Sci Technol 41 (11), 3934–3939. https://doi.org/10.1021/es062439i.
[47] Schleicher, N.J., Schafer, J., Blanc, G., Chen, Y., Chai, F., Cen, K., et al., 2015. Atmospheric particulate mercury in the megacity Beijing: spatiotemporal variations and source apportionment. Atmos Environ 109, 251–261. https://doi.org/10.1016/j.atmosenv.2015.03.018.
[48] Sherman, L.S., Blum, J.D., Keeler, G.J., Demers, J.D., Dvonch, J.T., 2012. Investigation of local mercury deposition from a coal-fired power plant using mercury isotopes. Environ Sci Technol 46 (1), 382–390. https://doi.org/10.1021/es202793c.
[49] Steffen, A., Schroeder, W., Bottenheim, J., Narayan, J., Fuentes, J.D., 2002. Atmospheric mercury concentrations: measurements and profiles near snow and ice surfaces in the Canadian Arctic during Alert 2000. Atmos Environ 36 (15–16), 2653–2661. https://doi.org/10.1016/s1352-2310(02)00112-7.
[50] Sun, G., Feng, X., Yang, C., Zhang, L., Yin, R., Li, Z., et al., 2020. Levels, sources, isotope signatures, and health risks of mercury in street dust across China. J Hazard Mater 392, 122276. https://doi.org/10.1016/j.jhazmat.2020.122276.
[51] Sun, G.Y., Sommar, J., Feng, X.B., Lin, C.J., Ge, M.F., Wang, W.G., et al., 2016. Mass-dependent and -independent fractionation of mercury isotope during gas-phase oxidation of elemental mercury vapor by atomic Cl and Br. Environ Sci Technol 50 (17), 9232–9241. https://doi.org/10.1021/acs.est.6b01668.
[52] Sun, L.M., Zhang, X.D., Zheng, J.Y., Zheng, Y.Q., Yuan, D.X., Chen, W.J., 2021. Mercury concentration and isotopic composition on different atmospheric particles (PM10 and PM2.5) in the subtropical coastal suburb of Xiamen Bay, Southern China. Atmos Environ 261 (118604). https://doi.org/10.1016/j.atmosenv.2021.118604.
[53] Sun, R., Enrico, M., Heimburger, L.E., Scott, C., Sonke, J.E., 2013. A double-stage tube furnace–acid-trapping protocol for the pre-concentration of mercury from solid samples for isotopic analysis. Anal Bioanal Chem 405 (21), 6771–6781. https://doi.org/10.1007/s00216-013-7152-2.

[54] Sun, R., Sonke, J.E., Liu, G., Zheng, L., Wu, D., 2014. Variations in the stable isotope composition of mercury in coal-bearing sequences: indications for its provenance and geochemical processes. Int J Coal Geol 133, 13–23. https://doi.org/10.1016/j.coal.2014.09.001.
[55] Sun, R.Y., Heimburger, L.E., Sonke, J.E., Liu, G.J., Amouroux, D., Berail, S., 2013. Mercury stable isotope fractionation in six utility boilers of two large coal-fired power plants. Chem Geol 336, 103–111. https://doi.org/10.1016/j.chemgeo.2012.10.055.
[56] Sun, R.Y., Sonke, J.E., Heimburger, L.E., Belkin, H.E., Liu, G.J., Shome, D., et al., 2014. Mercury stable isotope signatures of world coal deposits and historical coal combustion emissions. Environ Sci Technol 48 (13), 7660–7668. https://doi.org/10.1021/es501208a.
[57] Sun, R.Y., Streets, D.G., Horowitz, H.M., Amos, H.M., Liu, G.J., Perrot, V., et al., 2016. Historical (1850-2010) mercury stable isotope inventory from anthropogenic sources to the atmosphere. Elem: Sci Anthr 4, 1–15. https://doi.org/10.12952/journal.elementa.000091.
[58] Tang, Y., Wang, S.X., Wu, Q.R., Liu, K.Y., Li, Z.J., Zou, J., et al., 2019. Measurement of size-fractionated particulate-bound mercury in Beijing and implications on sources and dry deposition of mercury. Sci Total Environ 675, 176–183. https://doi.org/10.1016/j.scitotenv.2019.04.245.
[59] US EPA (2007). US EPA Method 7473, Mercury in Solids and Solutions by Thermal Decomposition, Amalgamation, and Atomic Absorption Spectrophotometry (US Environmental Protection Agency, Office of Solid Waste. (Washington, DC).
[60] Wang, C.J., Hui, F., Gao, Y., Wang, Z.W., Zhang, X.S., 2021. Temporal variation of speciated atmospheric Hg and characteristics of size-fractioned Hg-P at a suburban site in Shijiazhuang City, North China. Atmos Pollut Res 12 (12), 101253. https://doi.org/10.1016/j.apr.2021.101253.
[61] Wang, C.J., Wang, Z.W., Zhang, X.S., 2020. Two years measurement of speciated atmospheric mercury in a typical area of the north coast of China: sources, temporal variations, and influence of regional and long-range transport. Atmos Environ 228, 117235. https://doi.org/10.1016/j.atmosenv.2019.117235.
[62] Wang, J., Zhou, M., Liu, B.S., Wu, J.H., Peng, X., Zhang, Y.F., et al., 2016. Characterization and source apportionment of size-segregated atmospheric particulate matter collected at ground level and from the urban canopy in Tianjin. Environ Pollut 219, 982–992. https://doi.org/10.1016/j.envpol.2016.10.069.
[63] Wang, X., Luo, J., Yin, R.S., Yuan, W., Lin, C.J., Sommar, J., et al., 2017. Using mercury isotopes to understand mercury accumulation in the montane forest floor of the Eastern Tibetan Plateau. Environ Sci Technol 51 (2), 801–809. https://doi.org/10.1021/acs.est.6b03806.
[64] Wright, L.P., Zhang, L., Cheng, I., Aherne, J., Wentworth, G.R., 2018. Impacts and effects indicators of atmospheric deposition of major pollutants to various ecosystems - a review. Aerosol Air Qual Res 18 (8), 1953–1992. https://doi.org/10.4209/aaqr.2018.03.0107.
[65] Wu, Q.R., Wang, S.X., Li, G.L., Liang, S., Lin, C.J., Wang, Y.F., et al., 2016. Temporal trend and spatial distribution of speciated atmospheric mercury emissions in China during 1978-2014. Environ Sci Technol 50 (24), 13428–13435. https://doi.org/10.1021/acs.est.6b04308.
[66] Xu, H.M., Sun, R.Y., Cao, J.J., Huang, R.J., Guinot, B., Shen, Z.X., et al., 2019. Mercury stable isotope compositions of Chinese urban fine particulates in winter haze days: implications for Hg sources and transformations. Chem Geol 504, 267–275. https://doi.org/10.1016/j.chemgeo.2018.11.018.
[67] Xu, L.L., Chen, J.S., Yang, L.M., Niu, Z.C., Tong, L., Yin, L.Q., et al., 2015. Characteristics and sources of atmospheric mercury speciation in a coastal city, Xiamen, China. Chemosphere 119, 530–539. https://doi.org/10.1016/j.chemosphere.2014.07.024.
[68] Xu, L.L., Shi, J.Y., Chen, Y.P., Zhang, Y.R., Yang, M.R., Chen, Y.T., et al., 2021. Mercury isotopic compositions in fine particles and offshore surface seawater in a coastal area of East China: implications for Hg sources and atmospheric transformations. Atmos Chem Phys 21 (24), 18543–18555. https://doi.org/10.5194/acp-21-18543-2021.
[69] Yin, R., Feng, X., Chen, J., 2014. Mercury stable isotopic compositions in coals from major coal producing fields in China and their geochemical and environmental implications. Environ Sci Technol 48 (10), 5565–5574. https://doi.org/10.1021/es500322n.
[70] Yin, R., Feng, X., Hurley, J.P., Krabbenhoft, D.P., Lepak, R.F., Hu, R., et al., 2016. Mercury isotopes as proxies to identify sources and environmental impacts of mercury in sphalerites. Sci Rep 6 (1), 18686. https://doi.org/10.1038/srep18686.
[71] Yu, B., Fu, X.W., Yin, R.S., Zhang, H., Wang, X., Lin, C.J., et al., 2016. Isotopic composition of atmospheric mercury in China: new evidence for sources and transformation processes in air and in vegetation. Environ Sci Technol 50 (17), 9262–9269. https://doi.org/10.1021/acs.est.6b01782.
[72] Yu, B., Yang, L., Liu, H., Xiao, C., Bu, D., Zhang, Q., et al., 2022. Tracing the transboundary transport of mercury to the Tibetan plateau using atmospheric mercury isotopes. Environ Sci Technol 56 (3), 1568–1577. https://doi.org/10.1021/acs.est.1c05816.
[73] Yu, B., Yang, L., Wang, L.L., Liu, H.W., Xiao, C.L., Liang, Y., et al., 2020. New evidence for atmospheric mercury transformations in the marine boundary layer from stable mercury isotopes. Atmos Chem Phys 20 (16), 9713–9723. https://doi.org/10.5194/acp-20-9713-2020.
[74] Yu, G.Y., Qin, X.F., Xu, J., Zhou, Q., Wang, B., Huang, K., et al., 2019. Characteristics of particulate-bound mercury at typical sites situated on dust transport paths in China. Sci Total Environ 648, 1151–1160. https://doi.org/10.1016/j.scitotenv.2018.08.137.
[75] Zhang, H., Wang, Z.W., Wang, C.J., Zhang, X.S., 2019. Concentrations and gas-particle partitioning of atmospheric reactive mercury at an urban site in Beijing, China. Environ Pollut 249, 13–23. https://doi.org/10.1016/j.envpol.2019.02.064.
[76] Zhang, H., Yin, R.S., Feng, X.B., Sommar, J., Anderson, C.W., Sapkota, A., et al., 2013. Atmospheric mercury inputs in montane soils increase with elevation: evidence from mercury isotope signatures. Sci Rep 3, 3322. https://doi.org/10.1038/srep03322.
[77] Zhang, L., Wang, S.X., Wang, L., Hao, J.M., 2013. Atmospheric mercury concentration and chemical speciation at a rural site in Beijing, China: implications of mercury emission sources. Atmos Chem Phys 13 (20), 10505–10516. https://doi.org/10.5194/acp-13-10505-2013.
[78] Zhang, L.M., Wright, L.P., Blanchard, P., 2009. A review of current knowledge concerning dry deposition of atmospheric mercury. Atmos Environ 43 (37), 5853–5864. https://doi.org/10.1016/j.atmosenv.2009.08.019.
[79] Zheng, W., Chandan, P., Steffen, A., Stupple, G., De Vera, J., Mitchell, C.P.J., et al., 2021. Mercury stable isotopes reveal the sources and transformations of atmospheric Hg in the high Arctic. Appl Geochem 131, 105002. https://doi.org/10.1016/j.apgeochem.2021.105002.
[80] Zheng, W., Hintelmann, H., 2009. Mercury isotope fractionation during photoreduction in natural water is controlled by its Hg/DOC ratio. Geochim Et Cosmochim Acta 73 (22), 6704–6715. https://doi.org/10.1016/j.gca.2009.08.016.
[81] Zheng, W., Obrist, D., Weis, D., Bergquist, B.A., 2016. Mercury isotope compositions across North American forests. Glob Biogeochem Cycles 30 (10), 1475–1492. https://doi.org/10.1002/2015gb005323.